QUASI-EQUILIBRIUM FIGURES FOR AN INHOMOGENEOUS FLUID MASS, OF RIEMANN TYPE

J.U. Cisneros Parra

Facultad de Ciencias, UASLP, México

and

F.J. Martínez Herrera and J.D. Montalvo Castro

Instituto de Física, UASLP, México

RESUMEN

Se establece —tanto numérica como analíticamente— la imposibilidad de figuras exactas de equilibrio para una masa heterogénea de fluido ideal, autogravitante, compuesta por dos elipsoides confocales en que rigen condiciones de Riemann o Dedekind. El modelo, por lo tanto, rota como cuerpo rígido o bien está estático, en tanto que el fluido circula internamente con vorticidad uniforme. Por otro lado, numéricamente se llega a una solución aproximada (de cuasiequilibrio) si la vorticidad tiene una discontinuidad en la frontera que divide los elipsoides. Tal solución consiste en una serie de esferoides, siendo posible que el más interno evolucione hacia un elipsoide en, aproximadamente, la misma forma en que lo hacen los esferoides homogéneos. Sin embargo, esta evolución no se da para la masa externa, cuya superficie de presión cero tiende más bien a ser esférica. El caso que no conduce a ningún resultado es el de vorticidad común, que aquí fue tratado mediante una manipulación algebraica sencilla del teorema de Hamy.

Por un error numérico, y por desconocimiento nuestro de este teorema, que invalida la existencia de figuras para un modelo rotante compuesto de n capas elipsoidales confocales, dimos a conocer un resultado que hoy deseamos reconsiderar, según el cual eran posibles las figuras tipo Jacobi para $n = 2$.

ABSTRACT

We establish both, numerically and analytically, the non-existence of exact equilibrium figures for a self-gravitating heterogeneous mass of an incompressible fluid, made up of two confocal ellipsoids in which Riemann or Dedekind conditions prevail. The body, therefore, can be either rotating as a solid or else be static, but in both cases the fluid circulates internally with uniform vorticity. On the other hand, if a discontinuity in the vorticity applies at the boundary between the two ellipsoids, then an approximate (quasi-equilibrium) solution is numerically tractable. This solution appears as a series of spheroids, the internal one being able to evolve into an ellipsoid, in roughly the same way as the homogeneous spheroids do. However, this evolution is never reached by the external mass whose surface of zero pressure, instead, becomes nearly spherical. The case which admits no solution at all is that of common vorticity, here worked out by means of a simple algebraic manipulation of Hamy's theorem.

Because both, a numerical error, and our recent awareness of this theorem, which rules out the existence of figures for a rotating model made up of n confocal layers, we published a result asserting the existence of Jacobi-type figures for $n = 2$, and we reconsider also here this result.

1. INTRODUCTION

This paper deals with the subject of self-gravitating fluid equilibrium figures, for a model made up of two confocal ellipsoids of different densities, and is intended to have a dual purpose. In a first step, a past result of ours on a closely related matter is reconsidered; next, the problem of inhomogeneous equilibrium figures is focused on the Riemann and the Dedekind sequences. Therefore, the model of interest, which may or may not rotate as a solid has —in either case— internal motions of uniform vorticity. Originally, any result, and deduction thereof, was conceived to be justified on numerical grounds only. However, analytical means are also available to explain some aspects of our general result, and they will be embodied where possible. Throughout this work, references will be made to our two previous works on the subject, one on spheroids (Montalvo, Martínez, & Cisneros 1983, hereafter Paper I), and the other, which we wish to rectify here, on ellipsoids (Martínez, Cisneros, & Montalvo 1990, hereafter Paper II).

1.1. A Reconsideration of Paper II

In Paper II, the model was examined under Jacobi's viewpoint (Lyttleton 1951), so that the basic idea was to investigate if a Jacobi model could support a kind of atmosphere, also ellipsoidal in shape and provided, to avoid any dynamical effect with the same angular velocity. The conclusion to this problem, as worked out in Paper II, was that under certain restricted conditions, equilibrium figures were possible. This is, however, false since in actual fact no figures of this sort are possible at all. The reworking of this problem was motivated by a warning from a colleague (Chambat 1992) about the existence of an old —yet not widely known— theorem (Hamy 1887), ruling out our figures of Paper II. The scope of this theorem is far reaching, since it works for an ellipsoidal fluid made up of n confocal layers (each of different density) all of them rotating with common angular velocity. Our model, therefore, is Hamy's for $n = 2$, and in the Appendix we work, following closely Chambat's version for n layers, the proof of the theorem for $n = 2$. As for the origin of the incorrect solution exhibited in Paper II, it rests on a misapplication of the confocality condition at a certain step, involving the upper limit of the elliptic integrals E and F, in the first two terms of equations (12) and (13). The correct equations should have a subscript a, instead of n, in such terms. On the other hand, the theorem also holds if the model has one less axis (Tassoul 1978), as was independently shown by numerical means in one of the cases treated in Paper I.

Having accomplished the rectification of Paper II, we resume the task of investigating if equilibrium figures are possible when our body is modeled on Dedekind's or Riemann's, rather than on Jacobi's masses. A priori, Hamy's theorem when suitably modified, is likely to play an important role in the development of such problems and, accordingly, a solution implying equilibrium figures would be therefore forbidden; we will see that —to a great extent— this is so. The problem, therefore, would be finished at once. However, an approximate solution is tractable in the event that the vorticity has a discontinuity within the model and, although the concept of figure of equilibrium must be taken with some caution, we hope that our results may rise the interest of those who work in the field of stellar models (see e.g., Chambat 1994).

2. BOUNDARY CONDITIONS

Following the routine employed in § 2 of Paper II, we now give a short exposition of the Riemann procedures in terms, to simplify matters, of a homogeneous ellipsoidal mass. The composite model and its boundary conditions are next recalled.

2.1. Equilibrium Conditions

We recall that the kind of internal motion proposed by Dedekind can be represented (Chandrasekhar 1965a,b) by

$$v_1 = -q\zeta x_2, \qquad v_2 = (1-q)\zeta x_1, \qquad v_3 = 0; \tag{1}$$

where v_1, v_2, v_3 are the rectangular components of the fluid's tangential velocity, $\vec{\zeta} = \zeta\hat{k}$, is the vorticity, $\hat{k}$ the unit vector along the x_3 axis, and q is some constant which, in order to preserve the ellipsoidal boundary must be

$$q = \frac{a_1^2}{(a_1^2 + a_2^2)}. \tag{2}$$

The constraint of zero external pressure can be writen as

$$0 = B_{ell} + \frac{1}{2}(x_1^2 + x_2^2)[\omega^2 + \zeta\omega + q(1-q)\zeta^2] + \ constant \ , \tag{3}$$

where B_{ell} is the gravitational potential of an ellipsoid, assumed of semi-axes $a_1 > a_2 > a_3$, and $\vec{\omega} = \omega\hat{k}$ is its angular velocity. The equations yielding the Riemann figures follow then from the ratios of partial derivatives

$$\frac{\phi_{x_1}}{f_{x_1}} = \frac{\phi_{x_2}}{f_{x_2}} = \frac{\phi_{x_3}}{f_{x_3}} \ , \tag{4}$$

where ϕ stands for the right-hand side of equation (3), and f is the surface equation of the ellipsoid.

If the Dedekind (or Jacobi) sequence is desired, then ω (or ζ) is made zero in equation (3).

2.2. The Model

The above proceedings will be applied now to our model, whose interior (exterior) ellipsoid will be referred to as the 'nucleus' ('atmosphere'), writing a prefix n (a) to pertaining quantities; Figure 1 is a scheme of the model when it is endowed of a solid-body rotation plus an internal motion of different vorticities, as in the last of the four cases treated here. By its geometry, the model demands twice the application of pressure continuity: at the body's external surface and at the interface nucleus-atmosphere. One further constraint is that this last surface be free from surface tension, under the hypothesis that no flow of matter occurs across it (Landau & Lifshitz 1959). Let us write together these conditions at each point of the body's outer surface

$$p = 0 \, , \tag{5}$$

and at each point of the internal surface

$$p_n = p_a \, ; \tag{6}$$

we will define a new quantity ϕ', as the left-hand side of $p_n - p_a = 0$. To go one step further, we need the potentials at the surfaces of density discontinuity of the body. The potential is, of course, continuous at these surfaces.
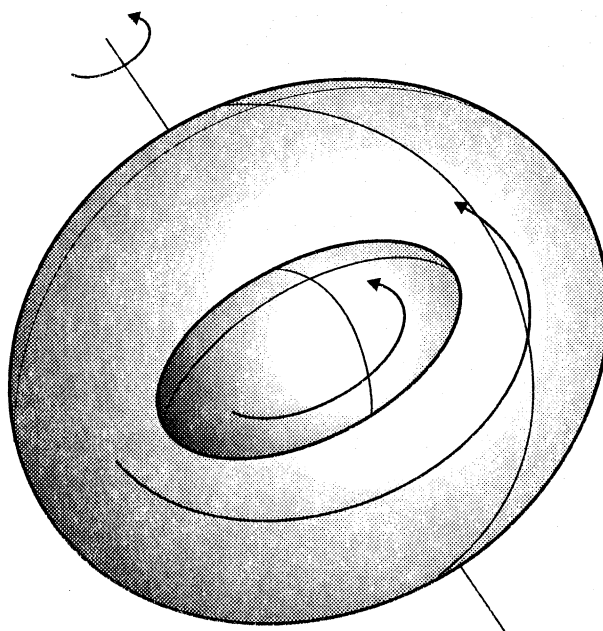

Fig. 1. The intended model. The large curved arrows indicate internal motions; the model itself is rotating as a solid body.

2.3. The Potentials

The derivation of the potential B_a at each point of the atmosphere is accomplished by following the sequence of steps indicated in Figure 1 of Paper I. We have

$$B_a = \pi G \Big[\rho_a a_{a_1} a_{a_2} a_{a_3} \int_0^\infty \frac{du}{\Delta_a} (1 - \sum \frac{x_i^2}{a_{a_i}^2 + u}) +$$

$$+ (\rho_n - \rho_a) a_{n_1} a_{n_2} a_{n_3} \int_\lambda^\infty \frac{du}{\Delta_n} (1 - \sum \frac{x_i^2}{a_{n_i}^2 + u}) \Big] , \qquad (7)$$

where the meaning of Δ_n, Δ_a, and λ is given in Paper II. The first integral of equation (7) represents an interior contribution from a homogeneous ellipsoid of density ρ_a, and so implies an excess of mass. This is compensated by the second integral, which is to account for an exterior contribution from a fictitious nucleus of density $\rho_n - \rho_a$; equation (7) also satisfies the potential at each point of the nucleus, B_n, letting $\lambda = 0$ in the lower limit of the second integral.

2.4. The Hypothesis of Confocality

As pointed out in Paper II, the problem of evaluating the partial derivatives in expression (4) gains a considerable simplification if the model is assumed as made up of confocal ellipsoids. The reason for this, we recall, is that the ellipsoidal coordinate λ is then constant all over the body's external surface, and zero all over the interface nucleus-atmosphere (see, however, the Appendix). With the convention that a subscript 1 (2) refers to the equatorial (meridional) direction, and e means eccentricity, the confocality relations are those given in § 2 of Paper II. As a consequence of those relationships the figures, if they exist, should agree with

$$e_{n_i} > e_{a_i} , \qquad i = 1, 2 , \qquad (8)$$

and

$$e_{n_1} / e_{a_1} = e_{n_2} / e_{a_2} . \qquad (9)$$

The nucleus, therefore, is polarly and equatorially more flattened than the atmosphere, and the eccentricities are not independent of each other. In the treatment that follows, e_{a_1} will be dropped out of the problem.

3. EQUATIONS AND RESULTS

We now proceed to deduce, from conditions (5) and (6), the equations that relate the body's physical and geometrical parameters for a number of different requirements. The angular velocity ω^2 and the vorticity $\zeta_{n,a}^2$, which will appear both normalized to $4\pi G \rho_a$, are given in terms of algebraic relationships among the eccentricities, the body's inhomogeneity degree $\epsilon [\equiv (\rho_n - \rho_a) \rho_a^{-1}]$, and the elliptic integrals of the first and second kind

$$F_n = \int_0^\alpha (e_{n_2}^2 - e_{n_1}^2 \sin^2 t)^{-1/2} e_{n_2} dt ,$$

$$E_n = \int_0^\alpha (e_{n_2}^2 - e_{n_1}^2 \sin^2 t)^{1/2} e_{n_2}^{-1} dt , \qquad (10)$$

$$F_a = \int_0^\beta (e_{a_2}^2 - e_{n_1}^2 e_{a_2}^2 e_{n_2}^{-2} \sin^2 t)^{-1/2} e_{a_2} dt ,$$

and

$$E_a = \int_0^\beta (e_{a_2}^2 - e_{n_1}^2 e_{a_2}^2 e_{n_2}^{-2} \sin^2 t)^{1/2} e_{a_2}^{-1} dt ,$$

where $\alpha = cos^{-1}(1 - e_{a_2}^2)^{1/2}$, and $\beta = cos^{-1}(1 - e_{n_2}^2)^{1/2}$ (Mac Millan 1958). For economy of space, however, only the set of equations corresponding to the case $\omega^2 = 0$, $\zeta_n^2 = \zeta_a^2$, will be fully displayed.

3.1. Case $\zeta_n^2 = \zeta_a^2$, $\omega^2 = 0$

In this and in the next case, the body's internal motion is assumed uniformly distributed throughout its volume, that is, the vorticity is homogeneous. There is, then, no need to affix a subscript to ζ. With this in mind, the quantities ϕ and ϕ', following each from conditions (5) and (6), become

$$\phi \equiv B_a + \frac{1}{2}(x_1^2 + x_2^2)\Big[\frac{a_{a_1}^2 a_{a_2}^2}{(a_{a_1}^2 + a_{a_2}^2)^2}\zeta^2\Big] + constant = 0\,, \tag{11}$$

and

$$\phi' \equiv \rho_n B_n - \rho_a B_a + \frac{1}{2}(x_1^2 + x_2^2)(\rho_n - \rho_a)\Big[\frac{a_{a_1}^2 a_{a_2}^2}{(a_{a_1}^2 + a_{a_2}^2)^2}\zeta^2\Big] + constant = 0\,. \tag{12}$$

Making expression (11) and the expression for the surface of the atmosphere to fit the ratios (4) there results

$$\frac{e_{n_2}^2(e_{n_2}^2 - e_{n_1}^2 e_{a_2}^2)}{(2e_{n_2}^2 - e_{n_1}^2 e_{a_2}^2)^2}Z^2 = \Big[\frac{(1 - e_{n_1}^2)^{1/2}(1 - e_{n_2}^2)^{1/2}(1 - e_{a_2}^2)}{e_{n_2}(e_{n_2}^2 - e_{n_1}^2)} - \frac{(1 - e_{n_1}^2)^{1/2}(1 - e_{n_2}^2)^{1/2}}{e_{n_2}e_{n_1}^2}\Big]\epsilon E_a$$

$$+ \frac{(1 - e_{n_1}^2)^{1/2}(1 - e_{n_2}^2)^{1/2}}{e_{n_2}e_{n_1}^2}\epsilon F_a + \Big[\frac{e_{n_2}(1 - e_{a_2}^2)^{3/2}(e_{n_2}^2 - e_{n_1}^2 e_{a_2}^2)^{1/2}}{e_{a_2}^3(e_{n_2}^2 - e_{n_1}^2)}$$

$$- \frac{e_{n_2}(e_{n_2}^2 - e_{n_1}^2 e_{a_2}^2)^{1/2}(1 - e_{a_2}^2)^{1/2}}{e_{n_1}^2 e_{a_2}^3}\Big]E_a + \frac{e_{n_2}(e_{n_2}^2 - e_{n_1}^2 e_{a_2}^2)^{1/2}(1 - e_{a_2}^2)^{1/2}}{e_{n_1}^2 e_{a_2}^3}F_a$$

$$- \frac{e_{a_2}(1 - e_{a_2}^2)^{1/2}(1 - e_{n_1}^2)^{1/2}(1 - e_{n_2}^2)^{1/2}(e_{n_2}^2 - e_{n_1}^2 e_{a_2}^2)^{1/2}}{e_{n_2}^2(e_{n_2}^2 - e_{n_1}^2)}\epsilon - \frac{(1 - e_{a_2}^2)(e_{n_2}^2 - e_{n_1}^2 e_{a_2}^2)}{e_{a_2}^2(e_{n_2}^2 - e_{n_1}^2)}\,, \tag{13}$$

$$\frac{e_{n_2}^2(e_{n_2}^2 - e_{n_1}^2 e_{a_2}^2)}{(2e_{n_2}^2 - e_{n_1}^2 e_{a_2}^2)^2}Z^2 = \Big[\frac{e_{n_2}(1 - e_{n_1}^2)^{1/2}(1 - e_{n_2}^2)^{1/2}(1 - e_{a_2}^2)}{(e_{n_2}^2 - e_{n_1}^2 e_{a_2}^2)(e_{n_2}^2 - e_{n_1}^2)} + \frac{e_{n_2}(1 - e_{n_1}^2)^{1/2}(1 - e_{n_2}^2)^{1/2}}{e_{n_1}^2(e_{n_2}^2 - e_{n_1}^2)}\Big]\epsilon E_a$$

$$- \frac{(1 - e_{n_1}^2)^{1/2}(1 - e_{n_2}^2)^{1/2}}{e_{n_2}e_{n_1}^2}\epsilon F_a + \Big[\frac{e_{n_2}^2(1 - e_{a_2}^2)^{3/2}}{e_{a_2}^3(e_{n_2}^2 - e_{n_1}^2 e_{a_2}^2)^{1/2}(e_{n_2}^2 - e_{n_1}^2)}$$

$$+ \frac{e_{n_2}^3(e_{n_2}^2 - e_{n_1}^2 e_{a_2}^2)^{1/2}(1 - e_{a_2}^2)^{1/2}}{e_{n_1}^2 e_{a_2}^3(e_{n_2}^2 - e_{n_1}^2)}\Big]E_a - \frac{e_{n_2}(e_{n_2}^2 - e_{n_1}^2 e_{a_2}^2)^{1/2}(1 - e_{a_2}^2)^{1/2}}{e_{n_1}^2 e_{a_2}^3}F_a$$

$$- \frac{2e_{a_2}(1 - e_{n_1}^2)^{1/2}(1 - e_{n_2}^2)^{1/2}(1 - e_{a_2}^2)^{1/2}}{(e_{n_2}^2 - e_{n_1}^2 e_{a_2}^2)^{1/2}(e_{n_2}^2 - e_{n_1}^2)}\epsilon - \frac{2e_{n_2}^2(1 - e_{a_2}^2)}{e_{a_2}^2(e_{n_2}^2 - e_{n_1}^2)}\,; \tag{14}$$

a similar procedure with expression (12), and the surface of the nucleus gives

$$\frac{e_{n_2}^2(e_{n_2}^2 - e_{n_1}^2 e_{a_2}^2)}{(2e_{n_2}^2 - e_{n_1}^2 e_{a_2}^2)^2}Z^2 = \Big[\frac{(1 - e_{n_2}^2)^{3/2}(1 - e_{n_1}^2)^{1/2}}{e_{n_2}(e_{n_2}^2 - e_{n_1}^2)} - \frac{(1 - e_{n_1}^2)^{1/2}(1 - e_{n_2}^2)^{1/2}}{e_{n_2}e_{n_1}^2}\Big]\epsilon E_n$$

$$+ \frac{(1 - e_{n_1}^2)^{1/2}(1 - e_{n_2}^2)^{1/2}}{e_{n_1}^2 e_{n_2}}\epsilon F_n + \Big[\frac{e_{n_2}(1 - e_{a_2}^2)^{1/2}(e_{n_2}^2 - e_{n_1}^2 e_{a_2}^2)^{1/2}(1 - e_{n_2}^2)}{e_{a_2}^3(e_{n_2}^2 - e_{n_1}^2)}$$

$$-\frac{e_{n_2}(1-e_{a_2}^2)^{1/2}(e_{n_2}^2-e_{n_1}^2e_{a_2}^2)^{1/2}}{e_{n_1}^2e_{a_2}^3}]E_a+\frac{e_{n_2}(1-e_{a_2}^2)^{1/2}(e_{n_2}^2-e_{n_1}^2e_{a_2}^2)^{1/2}}{e_{n_1}^2e_{a_2}^3}F_a$$

$$-\frac{(1-e_{n_1}^2)(1-e_{n_2}^2)}{(e_{n_2}^2-e_{n_1}^2)}\epsilon-\frac{(1-e_{n_2}^2)(e_{n_2}^2-e_{n_1}^2e_{a_2}^2)}{e_{a_2}^2(e_{n_2}^2-e_{n_1}^2)}, \qquad (15)$$

and

$$\frac{e_{n_2}^2(e_{n_2}^2-e_{n_1}^2e_{a_2}^2)}{(2e_{n_2}^2-e_{n_1}^2e_{a_2}^2)^2}Z^2=[\frac{(1-e_{n_2}^2)^{3/2}}{e_{n_2}(1-e_{n_1}^2)^{1/2}(e_{n_2}^2-e_{n_1}^2)}+\frac{e_{n_2}(1-e_{n_1}^2)^{1/2}(1-e_{n_2}^2)^{1/2}}{e_{n_1}^2(e_{n_2}^2-e_{n_1}^2)}]\epsilon E_n$$

$$-\frac{(1-e_{n_1}^2)^{1/2}(1-e_{n_2}^2)^{1/2}}{e_{n_2}e_{n_1}^2}\epsilon F_n+[\frac{e_{n_2}(1-e_{a_2}^2)^{1/2}(e_{n_2}^2-e_{n_1}^2e_{a_2}^2)^{1/2}(1-e_{n_2}^2)}{e_{a_2}^3(1-e_{n_1}^2)(e_{n_2}^2-e_{n_1}^2)}$$

$$+\frac{e_{n_2}^3(1-e_{a_2}^2)^{1/2}(e_{n_2}^2-e_{n_1}^2e_{a_2}^2)^{1/2}}{e_{n_1}^2e_{a_2}^3(e_{n_2}^2-e_{n_1}^2)}]E_a-\frac{e_{n_2}(1-e_{a_2}^2)^{1/2}(e_{n_2}^2-e_{n_1}^2e_{a_2}^2)^{1/2}}{e_{n_1}^2e_{a_2}^3}F_a$$

$$-2\frac{(1-e_{n_2}^2)}{(e_{n_2}^2-e_{n_1}^2)}\epsilon-\frac{(1-e_{n_2}^2)(e_{n_2}^2-e_{n_1}^2e_{a_2}^2)}{e_{a_2}^2(1-e_{n_1}^2)(e_{n_2}^2-e_{n_1}^2)}-\frac{e_{n_2}^2(1-e_{a_2}^2)}{e_{a_2}^2(e_{n_2}^2-e_{n_1}^2)}. \qquad (16)$$

It can be seen that the right-hand sides of equations (13)–(16) are just the right-hand sides of equations (12)–(15) of Paper II (after correction, see the discussion following the Introduction); the left-hand sides, on the other hand, are related according to

$$Z_i^2=\frac{(a_{a_1}^2+a_{a_2}^2)^2}{a_{a_1}^2a_{a_2}^2}\Omega_i^2=\frac{(2e_{n_2}^2-e_{n_1}^2e_{n_2}^2)^2}{e_{n_2}^2(e_{n_2}^2-e_{n_1}^2e_{a_2}^2)^2}\Omega_i^2. \qquad i=1\,\text{to}\,4. \qquad (17)$$

It is now apparent, from relation (17) and the procedure in the Appendix, that Hamy's theorem applies to this case. This is sufficient to warrant a null result, which the numerical analysis of the system of coupled equations (13)–(16) confirms.

In the cases that follow, only the left-hand side of the respective equilibrium equations, with modifications as required, will be handled not being necessary to write down their right-hand sides since they are exactly those of equations (13)–(16).

3.2. Case $\zeta_n^2=\zeta_a^2, \omega^2\neq 0$

We now review the preceding case for $\omega^2\neq 0$. Adding $\omega^2+\zeta\omega$ to the expression enclosed in square brackets, which is a factor of $\frac{1}{2}(x_1^2+x_2^2)$ in expressions (11) and (12), we obtain the equilibrium equations suitable for the current case. These are then just equations (13)-(16), with $\Omega^2+Z\Omega$ added to their left-hand sides.

If to the first (second) of these modified equations the third (fourth) one is subtracted, we arrive at the same contradiction as in the preceding case, which is as expected, since the additive terms $\Omega^2+Z\Omega$ cancel out exactly. Thus, a modified version of Hamy's theorem is once again met, and we conclude that equilibrium figures are forbidden, as our numerical approach confirms.

In reaching our conclusion that no figures can arise from the two revised cases, we have reverted to both, an analytical and a numerical method. Looking deeper into the model, let us see how an even more fundamental argument can be invoked. In so doing, we focus our attention on one of our basic pre-requisites, namely, that no matter can flow across the boundary surface nucleus-atmosphere. Indeed, this assumption was implicitly violated in our development of the problem, since the velocity of the fluid cannot be tangential to the outer boundary of the nucleus (Chambat 1994). If a perpendicular component of the velocity is present, the nucleus cannot preserve its shape, and the figure is unable to be formed at all.

It was seen, from the two previous cases that, if the vorticity is distributed homogeneously throughout the body, then no figures are possible because of a mathematical inconsistency of the equation systems. Next, these two cases are reanalyzed in the event that the vorticity changes abruptly at the interface nucleus-atmosphere. Thus, we have in mind to provide the body with an inhomogeneous distribution of vorticity, and so the quantity Z^2 will have to be provided of a subscript n, or a.

3.3. Case $\zeta_n^2 \neq \zeta_a^2, \omega^2 = 0$

In the current case the body, as a whole, remains static, while its internal currents behave as explained above. By such distribution of vorticity we mean that the semiaxes of the atmosphere (nucleus) fix the vorticity of the atmosphere (nucleus). Inserting the above considerations into the general equilibrium conditions (5) and (6), we have

$$\phi \equiv B_a + \frac{1}{2}(x_1^2 + x_2^2)[\frac{a_{a_1}^2 a_{a_2}^2}{(a_{a_1}^2 + a_{a_2}^2)^2}\zeta_a^2] + \; constant = 0 \,, \tag{18}$$

and

$$\phi' \equiv \rho_n B_n - \rho_a B_a + \frac{1}{2}(x_1^2 + x_2^2)[\rho_n \frac{a_{n_1}^2 a_{n_2}^2}{(a_{n_1}^2 + a_{n_2}^2)^2}\zeta_n^2 - \rho_a \frac{a_{a_1}^2 a_{a_2}^2}{(a_{a_1}^2 + a_{a_2}^2)^2}\zeta_a^2] + \; constant = 0 \,. \tag{19}$$

The left-hand sides of the pair of equations coming from ϕ can be reproduced from equations (13) and (14), with no more change than providing a prefix a to Z^2, while those coming from ϕ', on the other hand, modify into

$$\frac{(1 - e_{n_1}^2)}{(2 - e_{n_1}^2)^2}(\frac{\epsilon + 1}{\epsilon})Z_n^2 - \frac{e_{n_2}^2(e_{n_2}^2 - e_{n_1}^2 e_{a_2}^2)}{(2e_{n_2}^2 - e_{n_1}^2 e_{a_2}^2)^2}(\frac{1}{\epsilon})Z_a^2 \,. \tag{20}$$

In this and the next case no analytical means will be used. Numerical analysis —on the other hand— points to a solution or, rather to an approximate solution. We may shortly describe our approach, based on Newton's iterative method, writing the equilibrium equations as

$$G_i = (left\text{-}hand\ side) - (right\text{-}hand\ side) \quad i = 1\ to\ 4 \,, \tag{21}$$

which demands, for a solution to exist, the vanishing of G_i. For instance, if a pre-known figure, say a Jacobi one, is computed this way, we reach $G_i \sim 10^{-18}$. In the case that occupies us, instead, we consistently have $10^{-11} < G_i < 10^{-8}$, for a relatively wide range of ϵ. For $\epsilon \gtrsim 10$, however, G_3 and G_4 are $\gtrsim 10^{-8}$. Another important constraint shown by our general result, concerns the geometry itself of the figures, since none of them has such form as an oval-like nucleus with an oval-like atmosphere. Rather, the solution is mainly spheroidal in character for both nucleus and atmosphere, but the spheroidal nucleus can evolve into a well-defined ellipsoid if the nuclear vorticity is conveniently increased. However, if the nucleus evolves into an ellipsoid then the atmosphere or, more accurately, its surface of zero pressure becomes, roughly, spherical. This means that throughout our solution the equatorial section of the atmosphere is close to a circle. We remark that because of geometrical considerations the figures, at any rate, must fulfill $e_{n_1} > e_{a_1}$, and $e_{n_2} > e_{a_2}$ and, to that point, we must also expect that $e_{n_2} > e_{n_1}$ and $e_{a_2} > e_{a_1}$, since the x_3−axis is the axis about which the motions occur. Table 1 shows, for increasing ϵ, a cross-section of our general result, which proves valuable to be given in order of increasing e_{n_2}; these static models follow from equations (13)–(16) after the left-hand sides of the last two of them have been modified according to expression (19). For fixed ϵ, the table consists of three sections defining the geometry of the figures. We shall refer to the figures of ellipsoidal nucleus simply as ellipsoids, thus stressing somehow that this was the kind of geometry we were originally engaged with.

3.3.1. Spheroids

The family of spheroids satisfying the current conditions is, if we ignore its non-zero equatorial section, formally identical to that of Paper I, when the linking between $\zeta_{n,a}^2$ and $\omega_{n,a}^2$ occurs by the intermediary of proper geometrical constant factors. Therefore, this result will not be repeated in extended form here. Initially, when ϵ is still very low (not included in the table) and so the figures are quasi-homogeneous, the value of Z_a^2 tends to match that of Z_n^2, and we have the equivalent of a two-axes Maclaurin model. The numerical calculation of these last figures becomes difficult, however, since a cancellation of ϵ as a common factor took place in the first two equations, at a previous stage to their numerical analysis, which reflects in an irregular

108 CISNEROS PARRA, MARTÍNEZ HERRERA, & MONTALVO CASTRO

TABLE 1

PROPERTIES OF THE MODELS FOR CASE $\zeta_n^2 \neq \zeta_a^2, \omega^2 = 0^a$

Z_n^2	e_{n_1}	e_{n_2}	$10^4 Z_a^2$	$10^4 e_{a_1}$	e_{a_2}	Z_n^2	e_{n_1}	e_{n_2}	$10^4 Z_a^2$	$10^4 e_{a_1}$	e_{a_2}
$\epsilon = 0.1$						$\epsilon = 1$					
Spheroids						Transition Figures					
0.0700	0.0001	0.4447	567	0.684	0.3185	0.7983	0.0012	0.9263	94	1.700	0.1323
0.1057	0.0002	0.7500	421	0.930	0.2790	0.7983	0.0050	0.9276	3.3300	1.340	0.0250
0.1221	*0.0003*	*0.8692*	*3178*	*0.780*	*0.2429*	0.7983	0.0100	0.9276	1.2000	1.610	0.0150
0.1443	0.0005	0.9975	255	1.090	0.2179	Ellipsoids					
Transition Figures						0.7983	0.0500	0.9277	0.0219	1.070	0.0020
0.1221	0.0010	0.9585	79	1.250	0.1217	0.7983	0.1000	0.9280	0.0121	1.610	0.0015
0.1221	0.0050	0.9938	0.5330	0.500	0.0100	0.7990	0.2500	0.9300	0.0056	2.680	0.0010
0.1221	0.0100	0.9938	0.3400	0.800	0.0080	0.8138	0.5000	0.9380	0.0044	4.260	0.0008
Ellipsoids						0.9322	0.7500	0.9551	0.0055	6.280	0.0008
0.1220	0.0500	0.9931	0.0212	1.000	0.0020	3.2300	0.9675	0.9894	0.0067	7.820	0.0008
0.1220	0.1000	0.9931	0.0213	2.010	0.0020						
0.1222	0.2500	0.9933	0.0200	5.000	0.0020	$\epsilon = 1.5$					
0.1246	0.5000	0.9940	0.0044	4.030	0.0008	Spheroids					
0.1440	0.7500	0.9956	0.0056	6.000	0.0008	0.2750	0.0001	0.4712	868	0.690	0.3293
0.1443	0.7512	0.9957	0.0053	5.960	0.0009	0.8556	0.0002	0.8100	38	0.519	0.2617
0.2270	0.9000	0.9975	0.0063	7.210	0.0008	*1.0600*	*0.0002*	*0.9084*	*28*	*0.500*	*0.2295*
$\epsilon = 0.5$						1.1270	0.0002	0.9593	0.0251	0.585	0.2159
Spheroids						Transition Figures					
0.1500	0.0001	0.4382	1396	0.980	0.4212	1.0600	0.0012	0.9083	81	1.700	0.1233
0.3660	0.0002	0.8028	497	0.925	0.3008	1.0600	0.0050	0.9100	3.3300	1.370	0.0250
0.4797	0.0003	0.9438	204	0.622	0.1949	1.0600	0.0100	0.9083	0.3320	0.872	0.0079
0.4900	*0.0004*	*0.9617*	*155*	*0.660*	*0.1705*	Ellipsoids					
0.5613	0.0030	0.8127	0.5613	0.003	0.8127	1.0600	0.0500	0.9085	0.0190	1.040	0.0019
Transition Figures						1.0600	0.1000	0.9088	0.0019	2.090	0.0019
0.4797	0.0001	0.9512	84	1.300	0.1256	1.0610	0.2600	0.9117	0.0034	2.250	0.0008
0.4797	0.0050	0.9569	0.7700	0.630	0.0120	1.0800	0.5000	0.9217	0.0043	4.290	0.0008
0.4797	0.0100	0.9570	0.5100	1.020	0.0098	1.1270	0.6388	0.9318	0.0049	5.410	0.0008
Ellipsoids						1.2311	0.7500	0.9434	0.0054	6.280	0.0008
0.4797	0.0500	0.9571	0.0192	0.993	0.0019	5.0000	0.9745	0.9892	0.0065	7.780	0.0008
0.4797	0.1000	0.9572	0.0194	1.980	0.0019						
0.4802	0.2500	0.9584	0.0037	2.080	0.0008	$\epsilon = 2$					
0.4894	0.5000	0.9631	0.0043	4.150	0.0008	Spheroids					
0.5635	0.7500	0.9732	0.0054	6.160	0.0008	0.3680	0.0001	0.4889	737	0.940	0.3066
1.0000	0.9181	0.9869	0.0064	7.440	0.0008	0.7500	0.0003	0.6788	188	0.803	0.1849
$\epsilon = 1$						*1.2900*	*0.0003*	*0.8935*	*175*	*0.600*	*0.1800*
Spheroids						1.3500	0.0003	0.9815	151	0.600	0.1700
0.1900	0.0001	0.4515	613	0.600	0.2989	Transition Figures					
0.6144	0.0002	0.8030	244	0.530	0.2120	1.2900	0.0012	0.8932	91	1.750	0.1307
0.7983	*0.0003*	*0.9247*	*215*	*0.750*	*0.2000*	1.2900	0.0045	0.8925	3.2300	1.240	0.0246
0.8354	0.0004	0.9776	185	0.727	0.1856	1.3000	0.0100	0.8968	0.3390	0.882	0.0079

TABLE 1 (CONTINUED)

Z_n^2	e_{n_1}	e_{n_2}	$10^4 Z_a^2$	$10^4 e_{a_1}$	e_{a_2}	Z_n^2	e_{n_1}	e_{n_2}	$10^4 Z_a^2$	$10^4 e_{a_1}$	e_{a_2}
		$\epsilon = 2$						$\epsilon = 8$			
		Ellipsoids				*3.6900*	*0.0003*	*0.8433*	*50*	*0.111*	*0.0308*
1.2953	0.0500	0.8949	0.1110	2.550	0.0046	4.2300	0.0003	0.9387	27	0.259	0.0715
1.2953	0.1000	0.8953	0.1860	6.600	0.0059						
1.2965	0.2493	0.8983	0.0034	2.180	0.0008			Transition Figures			
1.3188	0.5000	0.9102	0.0043	4.340	0.0008	3.6900	0.0020	0.8438	65	0.265	0.1101
1.4974	0.7500	0.9352	0.0055	6.330	0.0008	3.6900	0.0050	0.8433	3.1500	1.450	0.0242
		$\epsilon = 4$				3.6900	0.0077	0.8433	0.1200	4.370	0.0047
		Spheroids						Ellipsoids			
0.4400	0.0002	0.4015	211	0.731	0.1739	3.6900	0.0500	0.8435	0.1120	2.720	0.0046
1.0000	0.0002	0.5982	387	0.800	0.2428	3.6900	0.1000	0.8442	0.0191	2.230	0.0019
2.1300	*0.0004*	*0.8659*	*217*	*0.820*	*0.1987*	3.6900	0.2500	0.8488	0.0034	2.320	0.0008
2.3400	0.0003	0.9254	0.0121	0.551	0.1500	3.7400	0.5000	0.8669	0.0044	4.550	0.0008
		Transition Figures						$\epsilon = 50$			
2.1300	0.0020	0.8649	105	3.180	0.1397			Spheroids			
2.1300	0.0050	0.8639	3	1.380	0.0240	5.9700	0.0001	0.4609	1210	0.450	0.2084
2.1400	0.0104	0.8663	0.1220	0.576	0.0048	13.0000	0.0001	0.6710	500	0.310	0.2085
		Ellipsoids				19.3400	0.0004	0.8160	165	0.780	0.1591
2.1300	0.0500	0.8654	0.1070	2.590	0.0045	*19.4400*	*0.0008*	*0.8182*	*171*	*1.580*	*0.1616*
2.1300	0.1000	0.8659	0.0190	2.190	0.0019			Transition Figures			
2.1370	0.2500	0.8699	0.0036	2.270	0.0079	19.4500	0.0010	0.8182	56	1.220	0.1000
2.1800	0.5248	0.8875	0.0047	4.740	0.0008	19.5000	0.0015	0.8187	19	1.080	0.0592
2.4300	0.7500	0.9176	0.0055	6.450	0.0008			Ellipsoids			
3.9000	0.9181	0.9603	0.0069	7.800	0.0008	19.4600	0.0400	0.8185	0.4470	4.470	0.0091
		$\epsilon = 8$				19.4600	0.1000	0.8194	0.0044	1.090	0.0009
		Spheroids				19.4700	0.2500	0.8248	0.0046	2.730	0.0009
1.0000	0.0002	0.4517	1249	1.320	0.2845	19.7100	0.5000	0.8461	0.0058	5.310	0.0009
3.8500	0.0003	0.8657	123	0.468	0.1500						

[a] Notation: $\epsilon + 1$ is the density ratio $\rho_n \rho_a^{-1}$; Z^2 refers to vorticity normalized to $\left(4\pi G \rho_a\right)^{-1}$; e_{n_1}, e_{n_2}, e_{a_1}, e_{a_2} are the equatorial (1) and meridional (2) eccentricities of the nucleus (n) and the atmosphere (a). Figures of bifurcation are in italics.

accuracy $(G_{1,2} \sim 10^{-7}, G_{3,4} \sim 10^{-13})$. It is also possible, as contradictory as it may seem, to calculate a homogeneous figure for $\epsilon \neq 0$. This occurs when the confocality condition reaches its limiting point (see this case for $\epsilon = 0.5$ in Table 1), because the nucleus grows so that its size becomes comparable to that of the atmosphere. We will focus our attention, and this will become clear as we proceed onwards, on spheroids which, besides being of high e_{n_2}, are also of low e_{a_2}. In terms of vorticities, these spheroids are of both, high Z_n^2 and low Z_a^2. The spheroidal family extends even for the range $-1 < \epsilon < 0$, where we have the mathematical fact that the figures are of both, $\rho_n < \rho_a$ and $Z_n^2 < Z_a^2$. These figures are not of physical interest.

3.3.2. Transition Figures

In order to deal with the ellipsoidal form for both, nucleus and atmosphere, a given spheroid must —in the first place— be provided of non-circular equatorial sections, that is, e_{n_1} and e_{a_1} must be substantially increased. One finds, however, that not all spheroids are susceptible to be so deformed; in fact, only a particular spheroid, for given ϵ, can have such changes and, moreover, only in e_{n_1}. As we have already emphasized, e_{a_1} remains close to zero throughout our solution. The particular spheroid has a remarkable polar flattening in its nucleus, such as one of those listed last in the section of spheroids of Table 1. Therefore, in order to accomplish our

aim, the series will continue to be described in the direction of increasing e_{n_1} which, in this second stage will comprise the range $10^{-3} < e_{n_1} < 10^{-2}$. These figures were isolated because they represent a sort of transition between the spheroids and the figures referred here as ellipsoidal. A transition figure, then, has a nucleus whose equatorial flattening is midway between spheroidal and ellipsoidal, and an atmosphere whose polar flattening is noticeable (although of low value). These figures are the last, in the sequence of Table 1, in showing a relatively important atmospheric fluid activity, they being of $Z_n^2 >> Z_a^2$. It will prove valuable, from here onwards, to notice that an increase of e_{n_1} is accompanied by a decrease, in roughly the same proportion, of e_{a_2}, the two other flattenings remaining, more or less, constant, i.e., e_{a_1} close to zero and e_{n_2} close to 0.9, or so. Also notice that, if we think of our model, the closest figure to it would be the first listed among the transition figures.

3.3.3. Ellipsoids

A look into the transition figures shows that we cannot still claim to have arrived at the ellipsoidal form, even for the nucleus. In order to deform one such figure into the ellipsoidal form for both, nucleus and atmosphere, an additional increase of at least three of its sections, namely, e_{n_1}, e_{a_1} and e_{a_2} is required, while a somewhat lower value of e_{n_2} would also be desirable. From our calculations it was noticed that —at least for the nucleus— the ellipsoidal form was not impossible, but such ellipsoids were restricted to be very flattened at the poles. Since spheroids of high nuclear polar flattening are not unusual we tried them, as a starting point, in order to increase the nuclear equatorial flattening, and we succeeded at it. The fact that the figures with ellipsoidal nucleus results from a spheroid of high nuclear flattening vaguely reminds us, if we ignore the atmosphere, of the bifurcation of the Jacobi sequence from the Maclaurin sequence, so that two figures, one spheroidal, the other ellipsoidal can have the same angular velocity. In our case, the duality of figures occurs according to Z_n^2, as it is easily deduced from Table 1. To stress this question Table 1 contains some of these double-valued figures. Figure 2 depicts how all these sequences, along with that of the spheroids of Paper I, branch-off from each other in a scheme provided of no axes. We may read Figure 2 as follows. From each point (e, Ω^2) of the Maclaurin sequence a branch (actually a continuum of branches) of the series of spheroids from Paper I departs, ϵ increasing as indicated. Likewise, from each point of each of these branches, the quasi-equilibrium spheroids of the current work emerge, the ellipsoidal figures bifurcating then from a certain point of these branches. Accordingly, the direction of increasing Z_n^2 would be as indicated. Figure 2 should not be taken too literally, since each series needs for its description of a different number of parameters; it merely provides us of a quick-mean to visualize global features. Let us continue with the description of the inhomogeneous ellipsoids in the direction of increasing e_{n_1}. For $0.05 < e_{n_1} < 0.25$, Z_n^2 and, correspondingly, e_{n_2}, remain essentially constant, while the atmospheric polar flattening diminishes rapidly losing, therefore, the low although significant value, it had in the transition figures; at the far right of this interval, Z_a^2 collapses down to a minimum value of order 10^{-7}; for $e_{n_1} > 0.25$, Z_a^2 increases slightly, but still within that order of magnitude. The polar flattening of the atmosphere decreases to a value comparable to that of the equatorial one which is, we recall, very low throughout the solution, say $\sim 10^{-4}$. Hence, the atmosphere looks more like a sphere, which is consistent with its very scarce fluid activity; thus, in these figures Z_a^2 is negligible in comparison with Z_n^2. We can understand, with the help of relation (9), our current results since, as two of the flattenings (e_{n_2} and e_{a_1}) remain essentially constant for whatever reasons, then if other (e_{n_1}) increases, another (e_{a_2}) must necessarily decrease. We must therefore abandon any hope of having an ellipsoidal atmosphere surrounding our ellipsoidal nucleus.
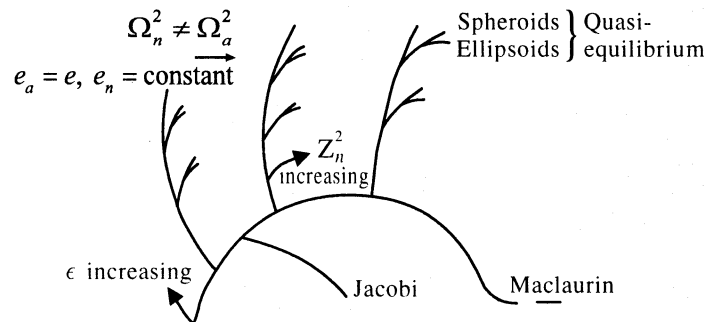

Fig. 2. Schematic diagram of the inhomogeneous sequences of this work, and that of Paper I. They are shown, in a conventional manner, branching-off the well known homogeneous sequences.
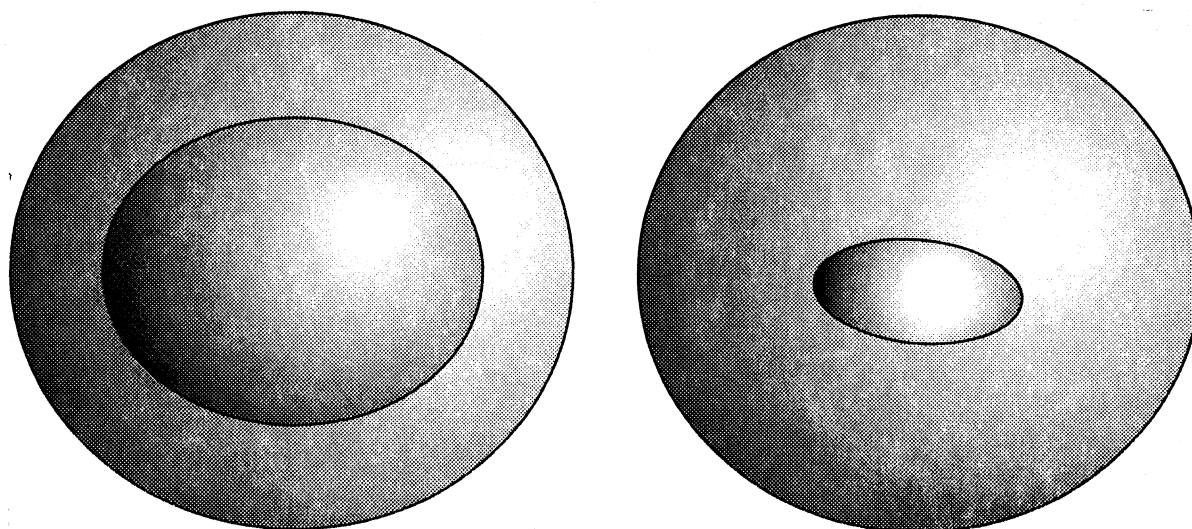
Fig. 3. The geometry of the obtained models is shown. (a) Spheroids, and (b) the figures with ellipsoidal nucleus.

Figure 3 illustrates the shape assumed by the figures, as they evolve from the spheroids, (a), into the ellipsoids, (b). The value of e_{a_2} that fits better into any nucleus of $e_{n_1} \gtrsim 0.25$ is about 8×10^{-4}, independently of ϵ, so that, after all, there is an unvanishing vestige of polar atmospheric flattening; the figures with this e_{a_2} value have $Z_a^2 \sim 10^{-7}$, and are of the highest possible degree of accuracy. Any attempt to provide a given ellipsoidal nucleus with an atmosphere more flattened at the poles than 8×10^{-4} results in lower accuracy. The fact that, for $e_{n_1} > 0.25$, and independently of ϵ, e_{a_2} settles to a fixed value, suggests that the gravitational coupling between the nucleus and the atmosphere becomes steady. However, this steadiness is not reached abruptly, rather, it begins to be patent as we proceed onwards from the bifurcation spheroid. As for the flattening e_{n_2}, it increases slightly as e_{n_1} increases, but it also decreases slightly if ϵ increases. Thus, the overall appearance of one of these figures is that of a small seed, surrounded by a nearly spherical, more tenuous, halo (see Figure 3b). Figure 4 gives Z_n^2 vs. ϵ, and it shows the regimes of these variables where the various kinds of figures occur.
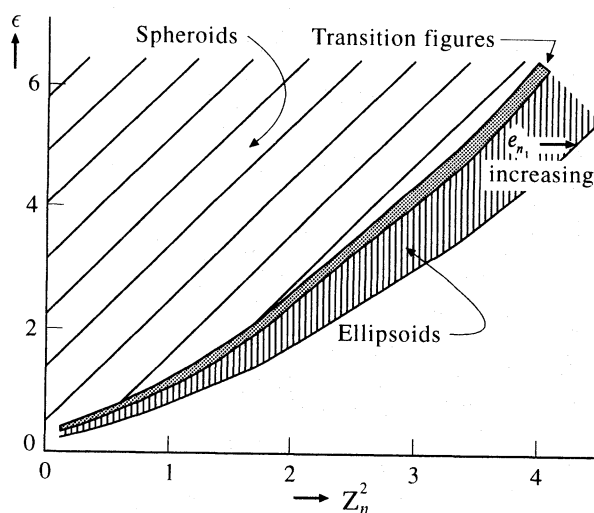

Fig. 4. This graph of ϵ vs. Z_n^2 shows the regimes of these variables where the various kinds of figures occur.

3.4. Case $\zeta_n^2 \neq \zeta_a^2$, $\omega^2 \neq 0$

To finish our study, let us examine the previous case in the event that the body is able to rotate as a solid (see Figure 1). We are looking, therefore, for inhomogeneous Riemann figures when the fluid's internal motion has a discontinuity in its vorticity at the surface of separation between the nucleus and the atmosphere; as we saw before, no such figures exist when that discontinuity does not apply. The quantities ϕ and ϕ' are now

$$\phi \equiv B_a + \frac{1}{2}(x_1^2 + x_2^2)[\omega^2 + \zeta_a\omega + \frac{a_{a_1}^2 a_{a_2}^2}{(a_{a_1}^2 + a_{a_2}^2)^2}\zeta_a^2] + constant = 0, \qquad (22)$$

and

$$\phi' \equiv \rho_n B_n + \frac{1}{2}(x_1^2 + x_2^2)$$

$$\times \{(\rho_n - \rho_a)\omega^2 + \rho_n \frac{a_{n_1}^2 a_{n_2}^2}{(a_{n_1}^2 + a_{n_2}^2)^2}\zeta_n^2 - \rho_a \frac{a_{a_1}^2 a_{a_2}^2}{(a_{a_1}^2 + a_{a_2}^2)^2}\zeta_a^2 + \rho_n\zeta_n\omega - \rho\zeta_a\omega\}. \qquad (23)$$

Therefore, the left-hand side of the two equations derived from expression (22) are

$$\Omega^2 + Z_a\Omega + \frac{e_{n_2}^2(e_{n_2}^2 - e_{n_1}^2 e_{a_2})}{(2e_{n_2}^2 - e_{n_1}^2 e_{a_2}^2)^2}Z_a^2, \qquad (24)$$

and those derived from expression (23) can be taken from expression (20) adding the terms

$$\Omega^2 + \frac{(\epsilon + 1)}{\epsilon}Z_n\Omega - \frac{1}{\epsilon}Z_a\Omega. \qquad (25)$$

TABLE 2

PROPERTIES OF THE MODELS FOR CASE $\quad \zeta_n^2 \neq \zeta_a^2$, $\omega^2 \neq 0^a$

Ω^2	e_{n_1}	e_{n_2}	Z_a	$10^4 Z_a^2$	$10^4 e_{a_1}$	e_{a_2}
$\epsilon = 1$ for $Z_n^2 = 0.7983$						
Spheroids						
0	0.0001	0.9269	0.0676	45.700	0.120	0.0925
0.00001	0.0001	0.9369	0.0613	37.000	0.120	0.0925
0.00005	0.0001	0.9316	0.0528	27.900	0.120	0.0916
0.00008	0.0001	0.9619	0.0488	23.800	0.120	0.0912
Transition Figures						
0	0.0012	0.9263	0.0965	0.009	1.720	0.1319
0.00001	0.0012	0.9364	0.0908	0.008	1.710	0.1328
0.00005	0.0012	0.9515	0.0771	0.006	1.54	0.1247
Ellipsoids						
0	0.3022	0.9312	0.0006	0.004	2.590	0.0008
0.00001	0.4829	0.9373	−0.0057	0.325	3.800	0.0007
0.00010	0.6040	0.9436	−0.0200	4.230	4.330	0.0007
0.00100	0.7468	0.9480	−0.0620	39	6.930	0.0009
0.01000	0.8921	0.9734	−0.1991	396	7.700	0.0008
0.05000	0.9805	0.9932	−0.4463	1992	8.300	0.0008

^{a} Notation: same as in Table 1, with $\Omega^2 \equiv \omega^2 (4\pi G\rho_a)^{-1}$, the angular velocity of the body.

The equations derived from conditions (22) and (23) are, as expected, satisfied by the particular value $\Omega^2 = 0$ and we have already discussed the figures. For $\Omega^2 \neq 0$, an approximate solution such as that meant in the previous case also applies. This means simply that the figures of Table 1 are able to rotate as a solid body, with the only difference that now the fluid circulation within the atmosphere can be retrograde, that is, Z_a can be negative. This fact, which for the figures having ellipsoidal nucleus begins to occur as soon as the angular velocity is hardly noticeable, allows these figures to rotate as a solid body, otherwise they could not do so, considering that their atmosphere cannot be other than nearly spherical. In other words the atmosphere, when the body rotates, retains its shape by virtue of the contrary effect which supposes a retrograde circulation. The nucleus, on the other hand, is not affected in its circulation as a result of increasing Ω^2 but its flattening, in particular the equatorial one, is severely increased. Thus, beginning with a static ellipsoid of Table 1 of fixed both, Z_n^2 and ϵ, a new set of ellipsoids is generated by increasing Ω^2 thus enlarging the sequence given in Table 1. Table 2 gives, for $\epsilon = 1$ and $Z_n^2 = 0.7983$, the rotating figures, where Ω^2 has been increased up to a value such that the equatorial flattening almost equals the polar one. This last flattening also increases as Ω^2 does, but at a much slower rate than e_{n_1}.

The authors wish to point out that the intervention of F. Chambat was decisive to unveil the error that altered the results of paper II.

APPENDIX

A PROOF OF HAMY'S THEOREM FOR OUR MODEL OF PAPER II

The proceedings of this Appendix follow closely the proof for n layers provided to us by F. Chambat who, in addition, proves that confocality is a necessity for relative equilibrium, rather than an *ad hoc* hypothesis. The proof, for $n = 2$, consists in reaching a contradiction upon subtraction of equation (12) from equation (14), after correction, of Paper II. However, it will prove convenient to resort to the integral version of such equations, which are

$$\frac{\omega^2}{2\pi G} = \rho_a a_{a_1} a_{a_2} a_{a_3} \int_0^\infty \frac{du}{\Delta_a}\left(\frac{1}{a_{a_1}^2 + u}\right) + (\rho_n - \rho_a)a_{n_1} a_{n_2} a_{n_3} \int_\lambda^\infty \frac{du}{\Delta_n}\left(\frac{1}{a_{n_1} + u}\right)$$

$$-\frac{a_{a_3}^2}{a_{a_1}^2}\left[\rho_a a_{a_1} a_{a_2} a_{a_3} \int_0^\infty \frac{du}{\Delta_a}\left(\frac{1}{a_{a_3}^2 + u}\right) + (\rho_n - \rho_a)a_{n_1} a_{n_2} a_{n_3} \int_\lambda^\infty \frac{du}{\Delta_n}\left(\frac{1}{a_{n_3}^2 + u}\right)\right],$$

and

$$\frac{\omega^2}{2\pi G} = \rho_a a_{a_1} a_{a_2} a_{a_3} \int_0^\infty \frac{du}{\Delta_a}\left(\frac{1}{a_{a_1}^2 + u}\right) + (\rho_n - \rho_a)a_{n_1} a_{n_2} a_{n_3} \int_0^\infty \frac{du}{\Delta_n}\left(\frac{1}{a_{n_1}^2 + u}\right)$$

$$-\frac{a_{n_3}^2}{a_{n_1}^2}\left[\rho_a a_{a_1} a_{a_2} a_{a_3} \int_0^\infty \frac{du}{\Delta_n}\left(\frac{1}{a_{a_3}^2 + u}\right) + (\rho_n - \rho_a)a_{n_1} a_{n_2} a_{n_3} \int_0^\infty \frac{du}{\Delta_n}\left(\frac{1}{a_{n_3}^2 + u}\right)\right];$$

taking the difference of these two equations we get

$$0 = (\rho_n - \rho_a)a_{n_1} a_{n_2} a_{n_3}\left[\int_0^\infty \frac{du}{\Delta_n}\left(\frac{1}{a_{n_1}^2 + u}\right) - \int_\lambda^\infty \frac{du}{\Delta_n}\left(\frac{1}{a_{n_1}^2 + u}\right)\right]$$

$$+\left(\frac{a_{a_3}^2}{a_{a_1}^2} - \frac{a_{n_3}^2}{a_{n_1}^2}\right)\rho_a a_{a_1} a_{a_2} a_{a_3} \int_0^\infty \frac{du}{\Delta_a}\left(\frac{1}{a_{a_3}^2 + u}\right) \qquad (26)$$

$$+\frac{a_{a_3}^2}{a_{a_1}^2}(\rho_n - \rho_a)a_{n_1} a_{n_2} a_{n_3} \int_\lambda^\infty \frac{du}{\Delta_n}\left(\frac{1}{a_{n_3}^2 + u}\right) - \frac{a_{n_3}^2}{a_{n_1}^2}(\rho_n - \rho_a)a_{n_1} a_{n_2} a_{n_3} \int_0^\infty \frac{du}{\Delta_n}\left(\frac{1}{a_{n_3}^2 + u}\right).$$

We now proceed as follows in equation (26): write a single integral, which we may call I_1, instead of the difference enclosed in square brackets; split the last integral into two, call them I_2 and I_3, where I_2 runs from 0 to λ, and I_3 runs from λ to ∞; iii) write together I_1 and I_2; iv) write together I_3 and the penultimate integral. After these steps, there results

$$0 = (\rho_n - \rho_a)a_{n_1}a_{n_2}a_{n_3}\left(\frac{a_{n_1}^2 - a_{n_3}^2}{a_{n_1}^2}\right)\int_0^\lambda \frac{du}{\Delta_n}\left(\frac{1}{a_{n_3}^2 + u}\right)$$

$$+\left(\frac{a_{a_3}^2}{a_{a_1}^2} - \frac{a_{n_3}^2}{a_{n_1}^2}\right)\rho_a a_{a_1}a_{a_2}a_{a_3}\int_0^\infty \frac{du}{\Delta_a}\left(\frac{1}{a_{a_3}^2 + u}\right) + \left(\frac{a_{a_3}^2}{a_{a_1}^2} - \frac{a_{n_3}^2}{a_{n_1}^2}\right)a_{n_1}a_{n_2}a_{n_3}\int_\lambda^\infty \frac{du}{\Delta_n}\left(\frac{1}{a_{n_3}^2 + u}\right). \quad (27)$$

The first term is positive since $\rho_n > \rho_a$ and $a_{n_1} > a_{n_3}$, while the second and third terms are each separately positive, since by confocality we have

$$\frac{a_{a_3}^2}{a_{a_1}^2} \geq \frac{a_{n_3}^2}{a_{n_1}^2}.$$

Thus, the right-hand side of equation (27) is positive, which is impossible, and the proof follows.

REFERENCES

Chambat, F. 1992, private communication
_____. 1994, A&A, 292, 76
Chandrasekhar, S. 1965a, ApJ, 141, 1043
_____. 1965b, ApJ, 142, 890
Hamy, M. 1887, Theśe de la Faculté des Sciences, Annales de l'Observatoire de Paris, 1889, Mémoires, 19
Landau, L.D., & Lifshitz, E.M. 1959, Course of Theoretical Physics: Fluid Mechanics (New York: Pergamon Press), p. 318
Lyttleton, R.A. 1951, The Stability of Rotating Liquid Masses (Cambridge: Cambridge Univ. Press), p. 37

MacMillan, W.D. 1958, Theoretical Mechanics: The Theory of the Potential (New York: Dover Publications), p. 60
Martínez, F.J., Cisneros, J., & Montalvo, D. 1990, RevMexAA, 20, 15
Montalvo, D., Martínez, F.J., & Cisneros, J. 1983, RevMexAA, 5, 293
Tassoul, J.L. 1978, Theory of Rotating Stars (Princeton: Princeton Univ. Press), p. 82

J.U. Cisneros Parra: Facultad de Ciencias, Universidad Autónoma de San Luis Potosí, Alvaro Obregón No. 64, San Luis Potosí, S.L.P., México. (cisneros@cactus.fc.uaslp.mx).
F.J. Martínez Herrera and J.D. Montalvo Castro: Instituto de Física, Universidad Autónoma de San Luis Potosí, Alvaro Obregón No. 64, San Luis Potosí, S.L.P., México.